Impact of Biofield Treatment on Physical, Structural and Spectral Properties of Antimony Sulfide

Mahendra Trivedi, Gopal Nayak, Shrikant Patil, Rama Mohan Tallapragada, Omprakash Latiyal

Industrial Engineering & Management

Trivedi et al., Ind Eng Manage 2015, 4:3
http://dx.doi.org/10.4172/2169-0316.1000165

Research Article Open Access

Impact of Biofield Treatment on Physical, Structural and Spectral Properties of Antimony Sulfide

Trivedi MK, Nayak G, Patil S*, Tallapragada RM and Latiyal O

[1]*Trivedi Global Inc,10624 S Eastern Avenue Suite A-969, Henderson, NV 89052, USA*

Abstract

Antimony sulfide (Sb_2S_3) has gained extensive attention in solar cells due to their potential as a low-cost and earth abundant absorber material. In solar cell absorber, the optoelectrical properties such as energy band gap and absorption coefficient of Sb_2S_3 play an important role, which have strong relationships with their crystal structure, lattice parameter and crystallite size.

Hence in the present investigation, Sb_2S_3 powder samples were exposed to biofield treatment, and further its physical, structural and spectral properties are investigated. The particle size analysis showed larger particle size and surface area after treatment. X-ray diffraction (XRD) analysis revealed polycrystalline orthorhombic structure with superior crystallinity in treated Sb_2S_3 along with significant changes in the lattice parameters, which led to changes in unit cell volume and density. XRD data analysis indicates that crystallite size was increased by around 150% in treated sample. In FT-IR spectra, strong absorption band was observed at 400-700cm^{-1}, which confirms the presence of Sb_2S_3. Further, the absorption peak intensity in IR spectra was significantly reduced after treatment that was probably due to change in metal sulphur dipolar interaction.

Keywords: Biofield treatment; Antimony sulfide; X-ray diffraction; FT-IR; Particle size; Surface area; Scanning electron microscopy

Introduction

Antimony Sulfide (Sb_2S_3) is a semiconductor ceramics belonging to V-VI group of periodic table, which have high thermo-electric power and photosensitivity. Sb_2S_3 has a wide range of commercial applications in microwave devices, optoelectronic devices and solar cell absorber [1-4]. Sb_2S_3 fulfils the optoelectronic properties to obtain an electronic band gap in the near-infrared region and the visible region, depending on its crystalline or amorphous nature [5]. Sb_2S_3 is an important photoconductive semiconductor in the polycrystalline form as orthorhombic crystal structure. The optoelectrical properties of Sb_2S_3 such as charge carrier transport mechanism, conduction, photoelectric properties makes it a promising material in solar energy industries as a light absorbing material. For solar cell absorber applications, the absorption coefficient and the energy band gap of Sb_2S_3 plays a crucial role. It is already reported [6-7] that higher absorption coefficient and lower energy band gap improves the performance of an absorber in the solar cell. Furthermore, the energy band gap in Sb_2S_3 is inversely proportional to its crystallinity [6] and the absorption coefficient of Sb_2S_3 is directly proportional to its crystallite size [7].

Recently, Sb_2S_3 powders have been synthesized by conventional methods such as hydrothermal treatment, solvo thermal reaction, sonochemical method and high energy milling [5]. The high energy milling has been frequently used by various researchers to produce nanocrystalline Sb_2S_3 [5]. In the milling process, energy was normally provided in the form of mechanical or chemical means. Additionally, in conventional milling process many parameters need to be controlled for cost reduction such as power, ball diameter, contamination, time, etc. Therefore, high energy milling through biofield treatment could be a cost effective approach which can effectively modulate the crystalline and physical properties.

Researchers all around the world have confirmed that the solid matter consist of energy and once this energy vibrates at a certain frequency, that gives physical, atomic and structural properties to the matter such as shape, size, texture, crystal structure, atomic weight, etc. Similarly, the human body also consists of vibratory energy particles like neutrons, protons, and electrons, and when these charged particles vibrate at certain frequency, an electrical impulse is generated. Consequently varying of these electrical impulses with time, cause generation of magnetic field as per Ampere-Maxwell-Law, which cumulatively form electromagnetic field [8]. Hence, the electromagnetic field generated from the human body is known as biofield. This biofield often vary from person to person based on their physiology and internal dynamic processes. Mr. Trivedi is known for his unique physiology and biofield, through which he has already caused changes in the atomic and physical characteristics in various fields such as material science [9-16], agriculture [17-19], microbiology [20-22], and biotechnology [23,24]. Further, in the field of material science, the said biofield has significantly changed the lattice parameter, surface area, crystallite size and particle size in metals [9], carbon allotropes [11], and ceramics [13,15].

In this paper, we report the impact of Biofield on Sb_2S_3 powder with respect to its structural, spectral and physical characteristics.

Experimental

Antimony sulfide (Sb_2S_3) powder used in the present investigation was purchased from Sigma-Aldrich, USA. Procured Sb_2S_3 powder was distributed into five equal samples. One sample was considered as control, and other four samples were exposed to Mr. Trivedi's biofield, referred herein as treated samples (T1, T2, T3, and T4). All samples

***Corresponding author:** Patil S, Trivedi Global Inc,10624 S Eastern Avenue Suite A-969, Henderson, NV 89052, USA, Tel: +1 602-531-5400; E-mail: publication@trivedieffect.com

Received June 02, 2015; **Accepted** July 15, 2015; **Published** July 17, 2015

Citation: Trivedi MK, Nayak G, Patil S, Tallapragada RM, Latiyal O (2015) Impact of Biofield Treatment on Physical, Structural and Spectral Properties of Antimony Sulfide. Ind Eng Manage 4: 165. doi:10.4172/2169-0316.1000165

were characterized by X-ray Diffraction, Scanning Electron Microscopy (SEM), Laser particle size analyzer, surface area analyzer (BET) and Fourier transform infrared spectroscopy (FT-IR) analysis.

Particle size analysis

Average particle size distribution and particle size were measured by Laser particle size analyzer SYMPATEC HELOS-BF, which had the detection range of 0.1-875 µm.

Surface area analysis

The surface area was measured by using surface area analyzer, SMART SORB 90 Brunauer-Emmett-Teller (BET) with a detection range of 0.1-1000 m^2/g.

X-ray diffraction

The atomic and structural level analysis was carried out using X-ray Diffraction (XRD), Phillips, Holland PW 1710. The copper anode with Nickel filter was used in this XRD instrument. The wavelength of radiation used in the instrument was 1.54056 Å and data provided by XRD was in the form of a chart of 2θ vs. intensity along with a table containing peak intensity counts, d value (Å), peak width (θ^0), relative Intensity (%). For the calculation of lattice parameter and unit cell volume PowderX software was used.

The crystallite size (L) was calculated using the formula: $L=k\lambda/(b\cos\theta)$

where k is the equipment constant (=0.94), and λ is the wavelength of radiation used. The molecular weight of a molecule is the sum of the atomic weight of all atoms, and the atomic weight is the sum of the total weight of protons, neutrons and electrons present in an atom. As number of molecules in a unit cell is fixed, so the weight of the unit cell was computed as the number of molecules present in a unit cell multiplied by the molecular weight of the molecules. The density was calculated as the weight of the unit cell divided by the volume of the unit cell. The percent change in lattice parameter, "a" was calculated as $[(a_t-a_c)/a_c] \times 100$ where ac and a_t are lattice parameter of control and treated powder samples respectively. The percentage change in all other parameters such as lattice parameter "b", unit cell volume, density, crystallite size were calculated in a similar manner.

Infrared spectroscopy

The IR spectra of samples were recorded by using Perkin Elmer, USA Fourier Transform Infrared (FT-IR) Spectrometer with frequency range of 300-4000/cm.

Scanning electron microscopy (SEM)

For surface morphology observation, Scanning electron microscopy (SEM), the JEOL JSM-6360 instrument was used.

Results and Discussion

Physical properties

The particle size and surface area analysis of control and treated Sb_2S_3 sample T1, T2, and T3 is shown in Figure 1. The treated sample T1, T2, and T3 were evaluated on 12th, 86th and 94th day after treatment respectively. The particle size analysis results showed that the average particle size d_{50} was decreased in treated Sb_2S_3 samples by 2%, 9.7% and 8.5% as compared to control in T1, T2, and T3 respectively. Nevertheless, the particle size d_{99} (size below which 99% particles are present) was increased in T1 by 12% and decreased in sample T2 and T3. Contrarily, the specific surface area was increased by 31% in sample T1 and then reduced by 31% in sample T3 as compared to control sample after treatment, though it was not changed in sample T2. The decrease in particle size was probably due to the fracturing of medium size particles into fine particles by energy milling that led to increased surface area in T1. The reduction in particle size and surface area in sample T3 was contrary to the fact i.e. smaller the particle size, larger the surface area. Thus it was postulated that, possibly the fresh surfaces of the particles were generated due to fracturing and agglomeration process through high energy milling. In order to get more insights about change in particle size and surface area, the powders were characterized by X-ray diffraction.

Atomic and structural properties

The XRD diffractogram of Sb_2S_3 is presented in (Figures 2a-2e). The XRD patterns of Sb_2S_3 confirms the orthorhombic crystal structure in control and all treated Sb_2S_3 samples as per JCPDS Card number 06-0474. From the XRD patterns, it was found that the peak intensity in treated sample T1 (Figure 2b) was increased along plane (200), (310) as compared to control (Figure 2a). Further the treated sample T2 also showed increased intensity (Figure 2c). This indicated that the crystallinity was enhanced in sample T1 and T2 that might be due to re-arrangement of the atoms in long range order through biofield. However the intensity of major peaks were not changed in sample T3 and T4 (Figures 2d and 2e).

Additionally, the crystal structure parameters were computed from the XRD patterns using PowderX software and analysis results are illustrated in Figures 3-6. It was observed that the lattice parameter "a" was increased from 11.28Å (control) to 11.45Å in T1 (Figure 3).

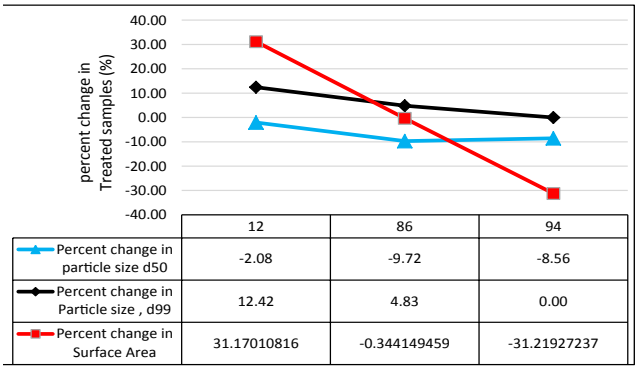

	12	86	94
Percent change in particle size d50	-2.08	-9.72	-8.56
Percent change in Particle size , d99	12.42	4.83	0.00
Percent change in Surface Area	31.17010816	-0.344149459	-31.21927237

Figure 1: Percent change in particle size and surface area of Sb_2S_3 with number of days after treatment.

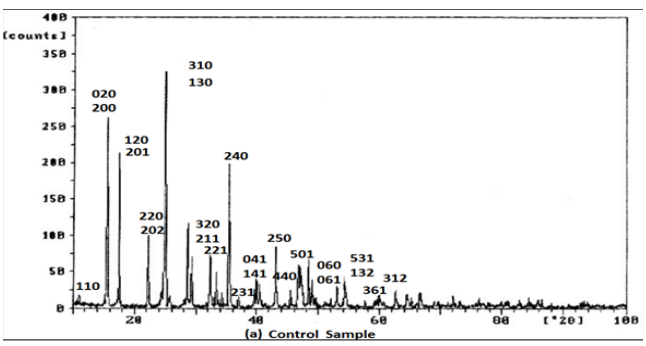

Figure 2a: XRD pattern of control Sb_2S_3 sample.

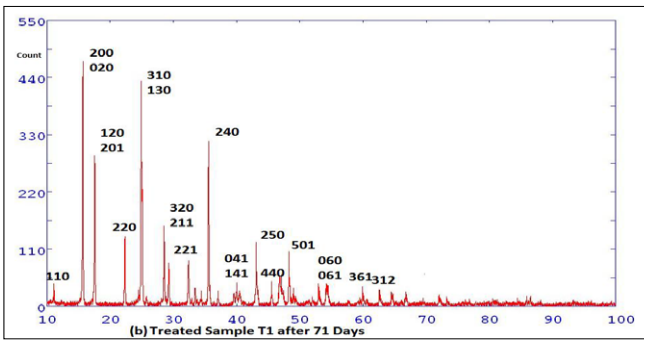

Figure 2b: XXRD pattern of treated Sb_2S_3 sample T1 (71 days after biofield treatment).

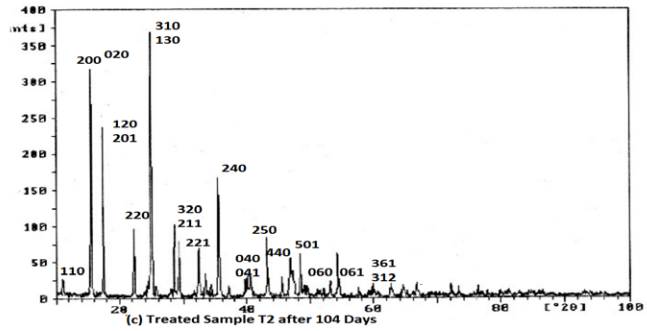

Figure 2c: XRD pattern of treated Sb_2S_3 sample T2 (104 days after biofield treatment).

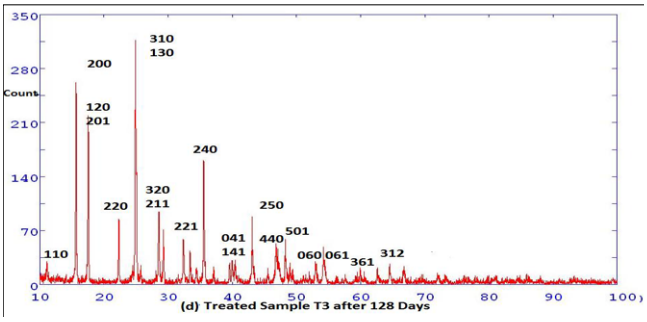

Figure 2d: XRD pattern of treated Sb_2S_3 sample T3 (128 days after biofield treatment).

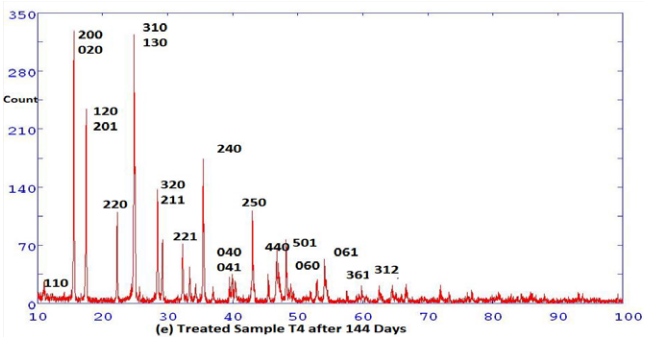

Figure 2e: XRD pattern of treated Sb_2S_3 sample T4 (144 days after biofield treatment).

Further, the results showed that on 71th day after treatment (T1), the lattice parameter "a" was increased significantly by 1.5% whereas lattice parameter "b" was decreased by 0.5% as compared to control. This causes the corresponding increase in volume by 0.63% that led to reduced density by -0.61% as compared to control (Figures 4-5). The lattice strain (change in lattice parameter) along "a" was positive and along "b" it was negative, which indicated that tensile stress was applied along "a" and compressive stress was applied along "b" during milling through biofield treatment, which further implies that the unit cell expanded along one side and compressed along another side. On 104th day after treatment (T2), no significant change was found in unit cell parameters. However, on 128th day (T3) unit cell parameter "a" was increased by 0.46% but parameter "b" was decreased by 0.37%, that led to no change in volume and density, since the volume increased through expansion of one side was compensated by compression in another side "b". This suggest that stresses may have been applied on unit cell along both sides, "a" and "b"; and direction and magnitude of these stresses varied with time after biofield treatment. Thus, the varying stresses on unit cell led to change the corresponding volume and density in treated samples. Moreover on 144th day after treatment (T4), no significant change was found in unit cell parameters. Further, the molecular weight changes were exactly opposite to the changes in the density as shown in Figure 6. This inverse relationship between molecular weight and density can be attributed to the change in proton to neutron ratio inside the nucleus. Furthermore the neutron to proton ratio can change if weak reversible nuclear level reaction occurs inside the nucleus. Thus, we presumed that biofield has transferred the energy in form of neutrinos that possibly cause this nuclear level reaction including proton-neutron to alter their ratio.

Additionally, the crystallite size was increased drastically by 150% in T1 with respect to control on 71th day after treatment (Figure 7). However, the crystallite size was increased in treated samples T2, T3 and T4 as well. This increased crystallite size was possibly due to

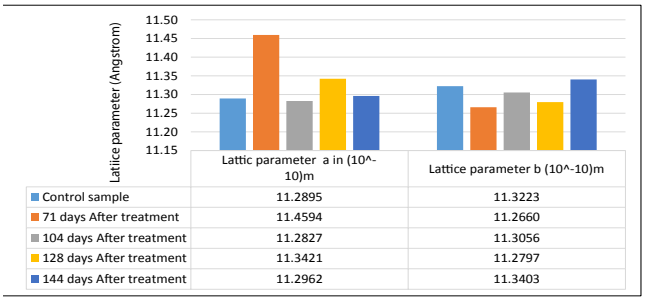

	Lattic parameter a in (10^-10)m	Lattice parameter b (10^-10)m
Control sample	11.2895	11.3223
71 days After treatment	11.4594	11.2660
104 days After treatment	11.2827	11.3056
128 days After treatment	11.3421	11.2797
144 days After treatment	11.2962	11.3403

Figure 3: Lattice parameters of control and treated Sb_2S_3 sample after certain number of days.

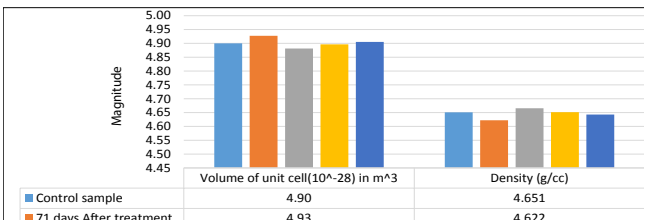

	Volume of unit cell(10^-28) in m^3	Density (g/cc)
Control sample	4.90	4.651
71 days After treatment	4.93	4.622
104 days After treatment	4.88	4.666
128 days After treatment	4.90	4.651
144 days After treatment	4.91	4.643

Figure 4: Unit cell volume and density of control and treated Sb_2S_3 sample after certain no. of days.

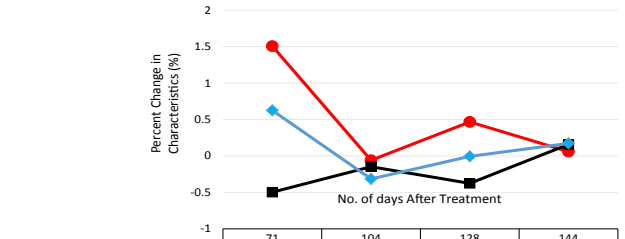

	71	104	128	144
Percent change in Lattice Parameter a	1.505475018	-0.059790282	0.466541358	0.059524548
Percent change in Lattice Parameter b	-0.497335356	-0.148290901	-0.376512276	0.15827117
Percent change in Volume of unit cell	0.63	-0.32	-0.01	0.17

Figure 5: Percent change in lattice parameters, unit cell volume of Sb_2S_3 with number of days after treatment.

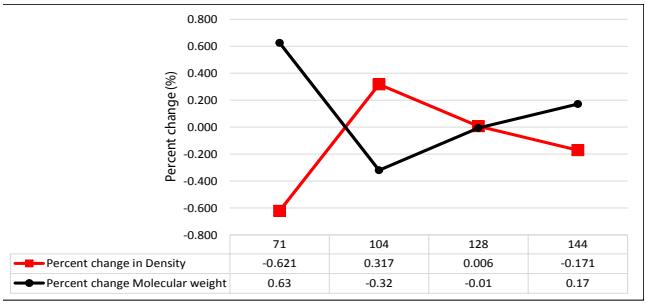

	71	104	128	144
Percent change in Density	-0.621	0.317	0.006	-0.171
Percent change Molecular weight	0.63	-0.32	-0.01	0.17

Figure 6: Percent change in density and molecular weight of $Sb_2S_3$with number of days after treatment.

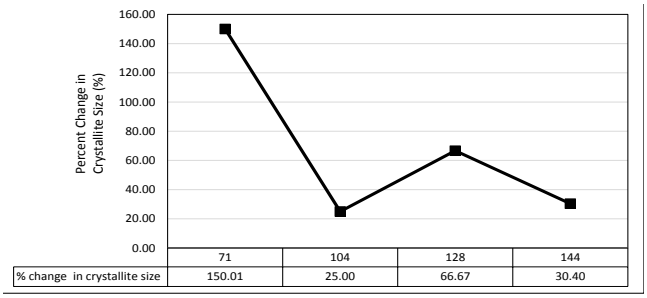

	71	104	128	144
% change in crystallite size	150.01	25.00	66.67	30.40

Figure 7: Percent change in crystallite size of Sb_2S_3 with number of days after treatment.

coalescence of several grains, due to movement of crystallite boundaries. Nevertheless the movement of crystallite boundaries could be possible if a large amount of energy (at least one-third of melting point) was supplied to the crystallite boundaries (similar to grain growth during sintering of powders at high temperature). Hence, it is hypothesized that energy might have been supplied to the Sb_2S_3 either directly through the biofield treatment or via the weak reversible nuclear reactions.

FT-IR spectroscopy

The FT-IR spectrum of control and treated Sb_2S_3 powder is shown in Figures 8a and 8b. The absorption peaks that were observed at 472, 518, 640/cm in control and 472, 516, 640/cm in T1 sample and 472, 516 ,644/cm in T2 sample were attributed to the presence of orthorhombic crystal structure of Sb_2S_3 [25,26]. However, no significant change was found in absorption peak positions in the fingerprint region of 400–700/cm in treated samples. Nevertheless the absorption band intensity was significantly reduced at 1112/cm in both treated samples, T1 and T2, which may be due to change in inter-atomic interaction [26]. The broad absorption bands in the region of 4000 to 2500/cm corresponds to the O–H stretch vibration peak due to the absorbed water.

Morphological studies

The surface morphology of Sb_2S_3 powder was studied using Scanning electron microscopy (SEM). The SEM micrographs of control and treated Sb_2S_3 powders are depicted in Figures 9a and 9b respectively. The SEM images of control Sb_2S_3 powder showed the irregular shape with internal agglomerated boundaries and sharp corners on the particles. Contrarily the treated Sb_2S_3 samples looks dense, homogenized with an increased agglomerated size. The increases in agglomerate size in treated samples have also supported the particle size results. The agglomerated Sb_2S_3 particles in treated samples were appeared as plate-like shape on all around the outer surfaces, which led to increase in surface area.

The structural, spectral and morphological studies revealed that the biofield treatment was acting on the structure, atoms, and their nuclei, which significantly affected the unit cell parameters, crystallite size, density, and molecular weight.

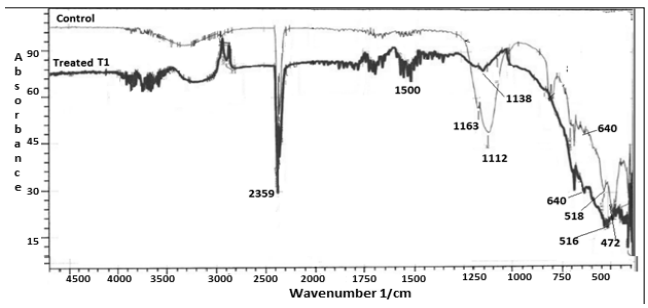

Figure 8a: FTIR spectra of control and treated Sb_2S_3 sample T1.

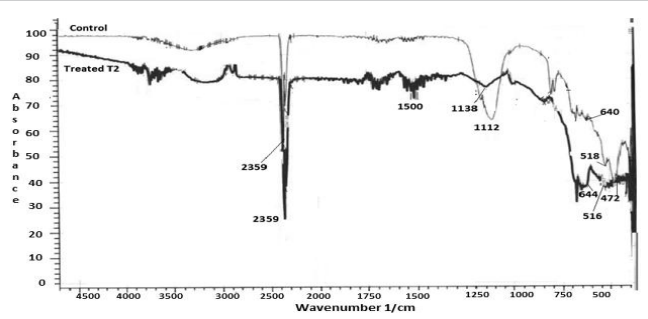

Figure 8b: FTIR spectra of control and treated Sb_2S_3 sample T2.

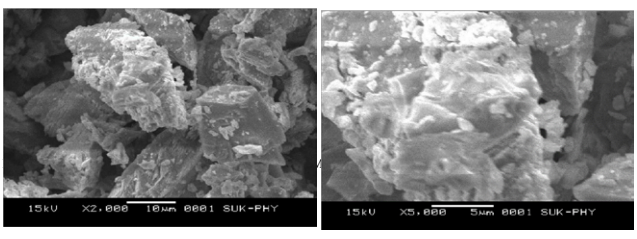

Figure 9a: SEM images of control Sb_2S_3samples at Magnification of 2000x and 5000x.

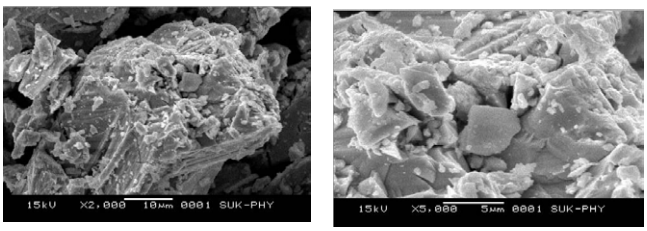

Figure 9b: SEM images of treatedSb_2S_3 samples at Magnification of 2000X and 5000X.

Conclusion

Herein we report the influence of biofield treatment on Sb_2S_3 powders, and its structural, spectral and physical properties are investigated. The significant increase as well as decrease in particle size and surface area was found in treated Sb_2S_3 powder, which may be due to agglomeration, fracturing and welding process caused by high energy milling induced through biofield treatment. The surface morphology study by SEM showed internal agglomerated boundaries and sharp angular particles in Sb_2S_3 powder that was probably due to internal friction and high energy impact during milling. Biofield has significantly altered the both lattice parameter: a and b simultaneously in orthorhombic crystal structure of Sb_2S_3 powders. This indicates that volumetric stress was probably generated through biofield treatment that resulted into changed density and volume. The significant changes in molecular weight asserted that biofield treatment acts at the atomic and nuclei level. The crystallite size was significantly increased by 150%, indicating the improved absorbance of Sb_2S_3 after treatment. Additionally, the crystallinity of Sb_2S_3 powder was also enhanced after biofield treatment that may have led to reduced gap in energy band. Therefore, the novel treated Sb_2S_3 powder can play an important role towards better solar cell absorber applications.

Acknowledgements

We thank Dr. Cheng Dong of NLSC, Institute of Physics, and Chinese academy of Sciences for supporting in using PowderX software for analyzing X-ray Diffraction results.

References

1. Tritt TM (1999) Thermoelectric materials: holey and unholy semiconductors. Science 283: 804-805.
2. Subramanian V, Siilvola E, Colpitts T, O'Quinn B (2001) Thin-film thermo-electric devices with high room-temperature figures of merit. Nature 413: 597-602.
3. Konstantatos G, Levina L, Tang J, Sargent EH (2008) Sensitive solution-processed Bi_2S_3 nanocrystalline photodetectors. Nano Letters 8: 4002-4006.
4. Rajpure KY, Bhosale CH (2000) Effect of composition on the structural, optical and electrical properties of sprayed Sb_2S_3 thin films prepared from non-aqueous medium. Journal of Physics and Chemistry of Solids 61: 561-568.
5. Dutková E, Sayagués MJ (2014) Proceeding of the International conference on mechanochemistry and Mechanical alloying, Poland, 22-26 June 2014. Mechanochemically Synthesized Nanocrystalline Sb_2S_3 Particles. 126: 943-946
6. Ismaila B, Mushtaqb S, Khan A (2014) Enhanced grain growth in the Sn doped Sb_2S_3 thin film absorber materials for solar cell applications. Chalcogenide Letters 11: 37-45.
7. Ezema FI, Ekwealor ABC (2007) Optical Properties and Structural Characterizations of Sb_2S_3 Thin Films Deposited by Chemical Bath Deposition Technique. Turkish Journal of Physics 31: 205-210.
8. Maxwell JC (1865) A dynamical theory of the electromagnetic field. Philosophical Transactions of the Royal Society of Londo 155: 459-512.
9. Trivedi MK, Tallapragada RR (2008) A transcendental to changing metal powder characteristics. Metal Powder Report 63: 22-28, 31.
10. Dabhade VV, Tallapragada RR, Trivedi MK (2009) Effect of external energy on atomic, crystalline and powder characteristics of antimony and bismuth powders. Bulletin of Materials Science 32: 471-479.
11. Trivedi MK, Tallapragada RR (2009) Effect of superconsciousness external energy on atomic, crystalline and powder characteristics of carbon allotrope powders. Materials Research Innovations 13: 473-480.
12. Trivedi MK, Patil S, Tallapragada RM (2012) Thought Intervention through Biofield Changing Metal Powder Characteristics Experiments on Powder Characterisation at a PM Plant. Future Control and Automation 173: 247-252.
13. Trivedi MK, Patil S, Tallapragada RM (2013) Effect of Biofield Treatment on the Physical and Thermal Characteristics of Vanadium Pentoxide Powders. Journal of Material Sciences and Engineering S11:001.
14. Trivedi MK, Patil S, and Tallapragada RM (2013) Effect of bio field treatment on the physical and thermal characteristics of Silicon, Tin and Lead powders. Journal of Material Sciences and Engineering 2: 125.
15. Trivedi MK, Patil S, and Tallapragada RM (2014) Atomic, Crystalline and Powder Characteristics of Treated Zirconia and Silica Powders. Journal of Material Sciences and Engineering 3: 144.
16. Trivedi MK, Patil S, Tallapragada RMR (2015) Effect of Biofield Treatment on the Physical and Thermal Characteristics of Aluminium Powders. Ind Eng Manage 4: 151.
17. Shinde V, Sances F, Patil S, Spence A (2012) Impact of Biofield Treatment on Growth and Yield of Lettuce and Tomato. Australian Journal of Basic and Applied Sciences 6: 100-105.
18. Sances F, Flora E, Patil S, Spence A, Shinde V (2013) Impact of Biofield Treatment on Ginseng and Organic Blueberry Yield. AGRIVITA Journal of Agricultural Science 35.
19. Lenssen AW (2013) Biofield and Fungicide Seed Treatment Influences on Soybean Productivity, Seed Quality and Weed Community. Agricultural Journal 8: 138-143.
20. Trivedi M, Patil S (2008) Impact of an external energy on *Staphylococcus epidermis* [ATCC -13518] in relation to antibiotic susceptibility and biochemical reactions - An experimental study. Journal of Accord Integrative Medicine 4: 230-235.
21. Trivedi M, Patil S (2008) Impact of an external energy on Yersinia enterocolitica [ATCC -23715] in relation to antibiotic susceptibility and biochemical reactions: An experimental study. The Internet Journal of Alternative Medicine 6.
22. Trivedi M, Bhardwaj Y, Patil S, Shettigar H., Bulbule A (2009) Impact of an external energy on *Enterococcus faecalis* [ATCC-51299] in relation to antibiotic susceptibility and biochemical reactions-An experimental study. Journal of Accord Integrative Medicine 5: 119-130.
23. Patil SA, Nayak GB, Barve SS, Tembe RP, Khan RR (2012) Impact of Biofield Treatment on Growth and Anatomical Characteristics of Pogostemon cablin (Benth.). Biotechnology 11: 154-162.
24. Altekar N, Nayak G (2015) Effect of Biofield Treatment on Plant Growth and Adaptation. Journal of environment and health sciences 1: 1-9.
25. Yu SH, Shu L, Wu YS, Qian YT, Xie Y, et al. (1998) Benzene-thermal synthesis and characterization of ultra-fine powders of antimony sulphide. Materials Research Bulletin 33: 1207-1211.
26. Subramanian S, Chithralekha P, Pathinettam PD (2010) Enhanced electrical response in Sb2S3 thin films by the inclusion of polyaniline during electrodeposition. Physica B 405: 925-931.

Citation: Trivedi MK, Nayak G, Patil S, Tallapragada RM, Latiyal O (2015) Impact of Biofield Treatment on Physical, Structural and Spectral Properties of Antimony Sulfide. Ind Eng Manage 4: 165. doi:10.4172/2169-0316.1000165